Estimating stream chemistry during the snowmelt pulse using a spatially distributed, coupled snowmelt and hydrochemical modeling approach

Noah P. Molotch,[1,2] Thomas Meixner,[3] and Mark W. Williams[4]

Received 10 October 2007; revised 20 August 2008; accepted 4 September 2008; published 26 November 2008.

[1] We used remotely sensed snow cover data and a physically based snowmelt model to estimate the spatial distribution of energy fluxes, snowmelt, snow water equivalent, and snow cover extent over the different land cover types within the Green Lakes Valley, Front Range, Colorado. The spatially explicit snowpack model was coupled to the Alpine Hydrochemical Model (AHM), and estimates of hydrochemistry at the basin outlflow were compared with the baseline AHM approach, which implicitly prescribes snowmelt. The proportions of total meltwater production from soil, talus, and rock subunits were 46, 25, and 29%, respectively, for the baseline simulation without our advanced snowmelt representation. Conversely, simulations in which the AHM was coupled to our distributed snowmelt model ascribed the largest meltwater production to talus (47%) subunits, with 37% ascribed to soil and 16% ascribed to rock. Accounting for these differences in AHM reduced model overestimates of cation concentration during snowmelt; modeled Ca^{2+} estimates explained 82 and 70% (P values < 0.01) of observations with and without the coupled model, respectively. Similarly, the coupled model explained more variability in nitrate concentrations, with 83 versus 70% (P values < 0.01) explained by the coupled and baseline models, respectively. Early snowmelt over talus subunits was not detected at the basin outflow, confirming earlier reports that deeper flow paths are needed in biogeochemical models of alpine systems. Realistic treatment of snowmelt within these models will allow efforts to improve understanding of flow paths and predict catchment response to increases in atmospheric deposition and climate change.

Citation: Molotch, N. P., T. Meixner, and M. W. Williams (2008), Estimating stream chemistry during the snowmelt pulse using a spatially distributed, coupled snowmelt and hydrochemical modeling approach, *Water Resour. Res.*, *44*, W11429, doi:10.1029/2007WR006587.

1. Introduction

[2] The timing and pattern of snowmelt plays a critical role in runoff generation and the geochemical and biogeochemical composition of stream water in alpine catchments [*Huth et al.*, 2004; *Liu et al.*, 2004; *Meixner et al.*, 2000; *Sickman et al.*, 2001]. Snowmelt is sensitive to climate variability as well as the effects of dust and black carbon on surface albedo [*Lundquist and Flint*, 2006; *McConnell et al.*, 2007; *Mote et al.*, 2005; *Painter et al.*, 2007]. Importantly, alpine systems are also sensitive to changes in atmospheric deposition, particularly deposition of acids and nitrogen (N) since N limits the productivity of most western United States montane ecosystems [*Fenn et al.*, 2003] and surface waters are poorly buffered against changes in pH [*Cumming et al.*, 1992; *Sullivan et al.*, 1990, 2005]. Past studies have shown fundamental links between biogeochemical fluxes and the timing and pattern of snowmelt. Some results have shown earlier melt increasing N retention in ecosystems [*Sickman et al.*, 2001], whereas others have indicated that the timing of snowpack accumulation and ablation can alter N retention as well [*Brooks et al.*, 1999; *Brooks and Williams*, 1999; *Brooks et al.*, 1998].

[3] Similarly, water flow paths and the geologic material it comes in contact with are critical controls on the neutralization of atmospherically deposited acidity and the resulting buffering of surface streams [*Clow et al.*, 1997; *Hooper and Christophersen*, 1992; *Liu et al.*, 2004; *Suecker et al.*, 2000]. Additionally, these and other studies have established links between the rate and location of snowmelt and the pathway and residence time of water in alpine catchments. Previous results in modeling alpine stream chemical composition have indicated that lack of knowledge of the path and residence time of water is a critical piece of information that needs to be improved on [*Campbell et al.*, 1995; *Huth et al.*, 2004; *Meixner et al.*, 2000, 2004; *Wolford and Bales*, 1996]. Since patterns of snow accumulation and snowmelt are susceptible to change in response to regional air temperature increases [*Mote et al.*, 2005], there

[1]Department of Civil and Environmental Engineering, University of California, Los Angeles, California, USA.
[2]Now at Water and Carbon Cycles Group, Jet Propulsion Laboratory, California Institute of Technology, Pasadena, California, USA.
[3]Department of Hydrology and Water Resources, University of Arizona, Tucson, Arizona, USA.
[4]Institute for Arctic and Alpine Research and Department of Geography, University of Colorado, Boulder, Colorado, USA.

0043-1397/08/2007WR006587$09.00

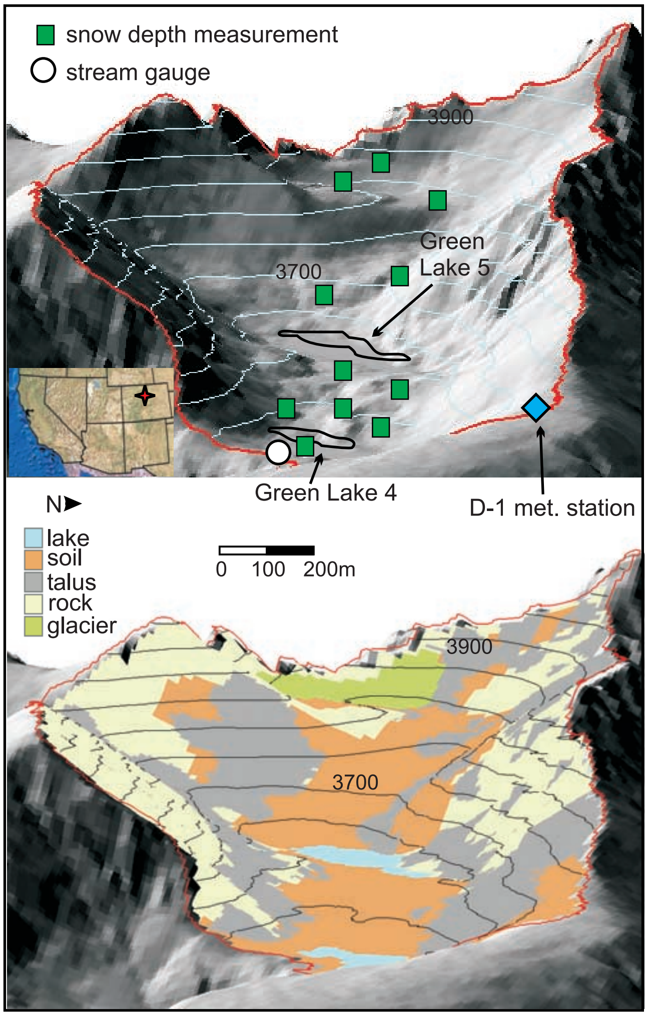

Figure 1. The Green Lake 4 watershed, shown in 3-D, looking up-valley to the west with land cover subunits. Grey shading represents a hill shade relief illuminated from the south. Contour interval is 25 m. The Saddle and C-1 sites are located approximately 3 and 7 km, respectively, to the east of D-1 (not shown).

is compelling science that indicates that advances in understanding feedbacks between hydrological and biogeochemical processes will increase our understanding of the susceptibility of alpine ecosystems to changes in climate and atmospheric deposition [*Meixner et al.*, 2000; *Melack et al.*, 1997; *Sickman et al.*, 2001].

[4] Despite the critical role of snowmelt, current models of alpine biogeochemistry make crude assumptions about the relationship of snowmelt to the temporal and spatial properties of runoff generation in alpine catchments [*Meixner and Bales*, 2003; *Meixner et al.*, 2000]. This crude representation of snowmelt results from difficulties associated with integrating robust physically based models of snowmelt with biogeochemical models of alpine systems [*Baron et al.*, 1994; *Hartman et al.*, 2007].

[5] In recent years there have been several critical advances in the measurement and modeling of the spatial distribution of three important hydrologic components of snowmelt: (1) the maximum snow water equivalent (SWE), (2) the snowmelt rate, and (3) the depletion of snow-covered area (SCA) [*Liston*, 1999]. First, our understanding of the physiographic controls on the accumulation of SWE has improved through the use of intensive field surveys of snowpack properties and statistical models [*Erickson et al.*, 2005]. Second, our ability to simulate snow-atmosphere energy exchange processes has improved with the evolution of temperature index approaches to physically based calculations of energy exchange [*Jordan*, 1991]. Third, advances in remote sensing have established the ability to estimate SCA at subpixel resolution [*Painter et al.*, 2003; *Rosenthal and Dozier*, 1996]. Integration of these techniques has improved our ability to quantify the temporal and spatial changes in snowmelt and snow-covered area [*Molotch et al.*, 2004; *Molotch and Bales*, 2006]. Incorporating these aforementioned advances into biogeochemical models is critical for expanding knowledge of feedbacks between climate and ecosystem function [*Brooks and Williams*, 1999; *Brooks et al.*, 1996; *Meixner and Bales*, 2003; *Sickman et al.*, 2001].

[6] Here we merge ground-based and remotely sensed snow observations within a spatially distributed, physically based snowmelt model to estimate the spatial and temporal distribution of SWE and snowmelt and to explicitly calculate the seasonal water balance. These estimates are then coupled to the Alpine Hydrochemical Model (AHM) to simulate discharge and hydrochemical fluxes at the catchment scale. This approach is used to address the following questions. (1) What is the spatial and temporal distribution of snow water equivalent and snowmelt over different land cover types in the Green Lake 4 (GLV4) catchment? (2) Does explicit representation of this variability improve simulations of hydrochemical fluxes? Previous applications of the AHM have relied on direct observations of streamflow to calculate the seasonal water balance. Thus, utilization of a model with an explicit calculation of the water balance will improve our ability to synthesize disparate sources of information, providing a diagnostic tool to improve understanding of important processes at the watershed scale. Further, the explicit representation of water balance terms in the coupled version of the model has the potential to extend the transferability of the AHM to ungauged basins and to regional-scale simulations.

2. Study Area

[7] This research was carried out in the 2.2-km^2 GLV4 watershed, Colorado (40°03′N, 105°35′W) (Figure 1), an alpine basin representative of the Colorado Front Range [*Caine*, 1995]. GLV4 ranges in elevation from 3550 to over 4000 m above sea level at the Continental Divide, with relatively equal areas of exposed bedrock (29%), talus (33%), and vegetated soils (29%). The 9-ha Arikaree glacier (4%) lies at the head of the catchment, upstream of Green lakes 4 and 5, which collectively cover 5% of the watershed area. Soils are located along the valley floor and are adjacent to the stream. The talus areas are generally located up-slope from the valley and are largely separated from the streams by soil subunits. Exposed bedrock areas in the watershed are located most prominently along the tops of ridges. The hydrology is dominated by a large winter snowpack which accounts for approximately 80% of total annual water input to the system [*Caine*, 1995]. The basin has a long history of biogeochemical and hydrological

studies dating back to the early 1980s [*Seastedt et al.*, 2004]. The site is ideal for studying hydrologic and ecological impacts of atmospheric deposition as air masses rise directly from low-elevation, upwind metropolitan, industrial, and agricultural centers, resulting in relatively elevated rates of atmospheric deposition [*Williams and Tonnessen*, 2000].

[8] There is a well-developed physical infrastructure at GLV4, including automated stream samplers, continuous discharge measurements, and climate stations along an elevational gradient. Niwot Ridge, the northern boundary of the Green Lakes Valley, is the site of other experimental areas, including a meteorological station, snow lysimeters, and a subnivean laboratory, all at the Saddle site at 3517 m (Figure 1). Long-term climate stations located at subalpine (C-1, 3048 m) and high alpine (D-1, 3749 m) sites have operated continuously since 1953.

3. Methods

[9] Two approaches to estimating hydrochemical fluxes were applied. The first approach followed the standard application of the AHM in which estimates of snowmelt are made on the basis of observed discharge and are uniformly distributed across snow-covered portions of the catchment as determined from a single aerial photograph at the beginning of the snowmelt season [*Meixner et al.*, 2000] (hereafter referred to as baseline simulations). The second approach used a coupled snowmelt-hydrochemical modeling scheme (hereafter referred to as coupled simulations) in which a time series of remotely sensed SCA data were merged into a spatially explicit, physically based energy and mass balance snowmelt model to reconstruct the spatial and temporal distribution of SWE and snowmelt throughout the snowmelt season [*Molotch et al.*, 2004]. The daily estimates of snowmelt from the coupled model were then routed through each land cover unit within the AHM. Here it is important to note that the coupled model does not require observations of streamflow for water balance calculations, whereas the baseline model effectively calibrates estimates of snowmelt to observed streamflow. Other than these differences in snowmelt calculation there are no differences between the baseline and coupled models in terms of model parameters, model structure, and initial conditions. The differences in snowmelt calculation do, however, have large implications with regard to model transferability to ungauged basins and to regional scales, as the coupled model can be developed for any seasonally snow-covered region without direct streamflow observations. Hydrochemical fluxes were evaluated for both approaches using a time series of water samples collected in the field and analyzed in the lab, affording an assessment of model performance for baseline versus coupled cases. Sections 3.1, 3.2, and 3.3 describe the snowmelt model, the hydrochemical model, and the forcings and observations.

3.1. Snowpack Energy and Mass Balance Model

[10] In the coupled modeling scenario we tracked the spatial and temporal distribution of snowmelt using a SWE reconstruction model in which remotely sensed snow cover data and energy balance modeling are used to estimate the spatial distribution of SWE and snowmelt [*Cline et al.*, 1998; *Molotch and Bales*, 2005, 2006; *Molotch et al.*, 2004].

[11] The SWE reconstruction model is based on a simple snowpack mass balance expression:

$$\mathrm{SWE}_n = \mathrm{SWE}_0 - \sum_{j=1}^{n} M_j, \tag{1}$$

where M_j is the melt flux at time step j, SWE_n is the SWE of the 30-m pixel at time step n, and SWE_0 is the initial SWE at the beginning of the snowmelt season. This mass balance expression is only valid in snow regimes where precipitation inputs during the snowmelt season are relatively insignificant relative to total winter snowfall; such an assumption is often valid in midlatitude alpine systems of the western United States [*Molotch and Bales*, 2005]. To obtain estimates of SWE_0, equation (1) is rearranged similar to that by *Cline et al.* [1998], when

$$\mathrm{SWE}_n = 0,\ \mathrm{SWE}_0 = \sum_{j=1}^{n} M_j. \tag{2}$$

[12] Here, SWE_0 is treated as each daily time step throughout the modeling period, encompassing the 1996 snowmelt season. Solving for SWE_0 is possible using remotely sensed snow cover observations which indicate the date that the snow-covered area equals zero. When SCA_n is equal to zero, SWE_n is also equal to zero, and at this time step n, the summation of the snowmelt flux can be converted to a linear depth of water that is equal to SWE_0. A real strength of this technique is that no estimate of initial SWE or any ground-based snow information is required and neither are any precipitation forcings. Hence, uncertainty in the spatial distribution of snowmelt and initial snow water equivalent is considerably reduced relative to conventional techniques which distribute sparse ground-based precipitation observations over topographically complex terrain. Rather, the reconstruction technique relies on a summation of the calculated melt flux over the remotely observed period of snow cover. For each time step the melt flux of each pixel was estimated as

$$M_j = \left(M_{p,j}\right)\left(\mathrm{SCA}_j\right), \tag{3}$$

where $M_{p,j}$ is the potential vertical snowmelt (i.e., linear depth), assuming continuous snow cover across the watershed. This potential vertical snowmelt is calculated using a single-layer physically based model with explicit representation of turbulent and radiative fluxes [*Cline et al.*, 1998; *Tarboton and Luce*, 1997]. These energy fluxes are directly transformed into water mass flux as estimates of sublimation and snowmelt. Remotely sensed observations of fractional SCA (30-m resolution) are used to define the area where snow-atmosphere energy exchange is modeled. Effectively, the vertical melt flux estimates are scaled by SCA (values range from 0 to 1) using pixel-specific snow cover depletion curves [*Molotch and Bales*, 2005, 2006; *Molotch et al.*, 2004]:

$$\mathrm{SCA}_j = \mathrm{SCA}_i - \left[\left(\mathrm{SCA}_i - \mathrm{SCA}_k\right)/\left(\sum_{i=1}^{n} M_{p,i} - \sum_{k=1}^{n} M_{p,k}\right)\right] \cdot \left[\sum_{i=1}^{n} M_{p,i} - \sum_{j=1}^{n} M_{p,j}\right], \tag{4}$$

where SCA_j is the estimated fractional SCA at time step j, SCA_i and SCA_k are remotely sensed fractional SCA values preceding and subsequent to time step j, respectively, and $\sum_{i=1}^{n} M_{p,i}$ and $\sum_{k=1}^{n} M_{p,k}$ are the potential vertical melt flux summation (or cumulative potential snowmelt) values corresponding to the remote sensing acquisition time steps i and k, respectively.

[13] We evaluated the spatial patterns of coupled model SWE estimates using "true" SWE distribution patterns from a complimentary study within the basin [*Erickson et al.*, 2005]. These complimentary estimates are based on 7 years (1997–2003) of field-based snow depth observations and an interpolation scheme in which snow depth is distributed as a random function that can be decomposed into a deterministic trend and a stochastic residual on the basis of elevation, slope, potential radiation [*Dozier*, 1980], an index of wind sheltering [*Molotch et al.*, 2005; *Winstral et al.*, 2002], and an index of wind drifting. Field-based observations to drive this interpolation model were not available for the water year studied here (i.e., 1996). Hence, we compared our results with snow distribution patterns from 1999 which are based on persistent spatial patterns of estimated snow depth from the analysis of *Erickson et al.* [2005]. These estimates represent the best approximation of the typical spatial pattern of snow depth in the basin. We recognize that an explicit evaluation against observations collected during the modeling period would be preferable, but detailed snow data collected in the GLV4 during the 1996 snowmelt season are not available. Notwithstanding, the persistent topographic controls on snow distribution patterns within the basin [*Erickson et al.*, 2005] make comparisons with other water years feasible.

[14] To avoid misinterpretation of model results, we used observations of discharge from the basin as a secondary metric of model performance. Streamflow incorporates the combined processes of snowmelt, sublimation, groundwater recharge, and evapotranspiration, integrated over a range of conditions throughout the basin.

[15] The benefit of the reconstruction model is that remotely sensed data can be used to update model snowpack state variables. In between aircraft overpasses, when SCA observations are unavailable, the physical representation of energy and mass transformations can be used to track changes in snowpack state, calculate snowmelt, and characterize the hydrology over the different subunits within the hydrochemical model.

3.2. Hydrochemical Model

[16] The AHM was designed for simulating hydrochemical fluxes in mountainous catchments using a lumped conceptual approach where the basin is partitioned into different terrestrial subunits (i.e., soil, rock, and talus), with a single stream subunit. Digitized soil maps were used to define the zones of soil, rock, and talus [*Meixner et al.*, 2000]. The model structure for the Green Lakes Valley included a rock subunit, a soil subunit, two talus subunits, and stream and lake subunits. The two talus subunits were necessary to represent both the widespread talus-dominated areas and the Arikaree glacier. Runoff from rock subunits was routed onto talus and subsequently to soil subunits prior to entering the stream. Within each terrestrial subunit, unique compartments are assigned for snowpack, snowpack-free water, snowmelt, surface runoff, and a range of soil horizons depending on subunit type (e.g., for rock subunits the number of soil horizons is zero). Stream subunits are disconnected from terrestrial processes, and their model compartments are limited to the snowpack, snowpack-free water, snowmelt, stream ice, and streamflow. Hydrologic processes are modeled separately from geochemical processes, affording easy coupling to the snowmelt model described in section 3.1. Hydrologic processes represented include infiltration into soils on the basis of hydraulic properties, drainage of these soils to streams on the basis of hydraulic conductivity, and unsaturated soil drying. Geochemical processes represented include ion elution from snowpacks, ion exchange, mineral weathering and equilibrium precipitation, and dissolution. Nitrogen biogeochemical processes affecting ammonium and nitrate are represented to handle the acid base implications of transformations. This process representation is simplistic in that it empirically accounts for removals, additions, and transformations of nitrogen species but does not robustly represent soil biogeochemical processes. Geochemical and biogeochemical reactions only occur in the soil compartments of the soil and talus subunits. Other compartments are mass balance storages for water and chemicals. A detailed description of the AHM can be found in the work by *Wolford and Bales* [1996], and specific application of the baseline approach to the GLV4 can be found in the work by *Meixner et al.* [2000].

[17] A unique attribute of the AHM is its multiple subunit structure that then parses each terrestrial subunit into snow-covered and snow-free areas, as the snow-free areas do not receive snowmelt once they become snow-free. Hence, surface contributions of these snow-free areas to basin outflow chemical fluxes are minimal. Thus, the major difference between the baseline and coupled simulations derives from the representation of snow cover depletion and snowmelt magnitude over each subunit in the basin. Baseline AHM simulations used a curve-fitting algorithm to estimate daily snowmelt values, constrained by observed discharge and a single SCA observation at the beginning of the snowmelt season. Conversely, in the coupled simulations an energy and mass balance snowmelt model is used to prescribe the magnitude of snowmelt and to estimate snow cover extent on each subunit. In this regard, snowmelt and SCA estimates of the coupled simulation were tracked on a daily basis (i.e., averages of hourly snowmelt simulations) and daily snowmelt estimates were overlaid on the soil, talus, and rock areas represented in the AHM. Snowmelt input to the terrestrial subunit was then treated as occurring only on the snow-covered portion of the subunit.

[18] Water balance calculations were required for the baseline simulations to convert observed streamflow to estimates of snowmelt. Within these calculations, a constant mean value of evapotranspiration based on field measurements from previous studies [*Meixner et al.*, 2000] was used within the AHM. Potential evapotranspiration (PET) during the winter period was set to 0.66 and 1.3 mm d^{-1} in winter and summer, respectively. Because of the absence of detailed sublimation data, potential sublimation was set to 75% of the PET values as per previous studies in the Emerald Lake catchment [*Wolford and Bales*, 1996]. Actual evaporation is

calculated by the model from soil and talus surfaces on the basis of a parameterized fraction of PET. In the simulations performed here, evaporation from soil was set equivalent to PET, and talus evaporation was set to 0.9 of PET, following *Meixner et al.* [2000]. Note that in the coupled simulations, these water balance calculations are not required as snowmelt is estimated explicitly.

3.3. Forcings and Observations

3.3.1. Hydrometeorological Forcing Data

[19] Hourly observations of incoming solar radiation, temperature, relative humidity, and wind speed from the Saddle site were used to force snowmelt simulations; information on instrument models and error are reported by *Williams et al.* [1999]. Observations from the D-1 and C-1 meteorological stations were used to establish elevational lapse rates, which were used in combination with a 10-m digital elevation model to extrapolate meteorological observations across the catchment [*Daly et al.*, 1994; *Thornton et al.*, 1997; *Willmott and Matsuura*, 1995]. Lapse rates were determined on an hourly basis for both temperature and wind speed. Surface roughness (0.0005 m) and other assumptions were consistent with those by *Jordan* [1991]. Precipitation quantity was recorded continuously at D-1 with a Belfort gauge shielded by a snow fence and an alter shield to improve gauge catch efficiency during windy periods. Total precipitation during water year 1996 was slightly above normal, at 1200 mm compared to the 50-year mean of 1000 mm. Rainfall contributed approximately 10% of the annual precipitation as measured at D-1. Spatially explicit estimates of precipitation type were classified as rain or snow on a per pixel basis across the catchment using a threshold temperature of 0°C. In the extrapolation of these meteorological observations there are inherent uncertainties associated with the representativeness of the observations made on Niwot Ridge versus unmeasured areas within the Green Lakes Valley. With regard to precipitation, however, it is important to note that the coupled approach to estimating SWE distribution does not require precipitation observations. Continuous discharge measurements recorded at the outflow of GLV4 indicated that annual discharge in 1996 was about 100% of the 20-year average [*Liu et al.*, 2004].

[20] TOPORAD [*Dozier*, 1980; *Dozier and Frew*, 1990] was used to model hourly clear-sky incoming solar radiation for each 10-m pixel within each of the six modeling domains. Incoming solar radiation in the visible (0.3–0.7 μm), near infrared (0.7–1.2 μm), and middle infrared (1.2–3.5 μm) were calculated separately and then integrated; a root mean square error of 55.93 W m^{-2} was determined from observations of solar radiation. Snow surface albedo was parameterized on the basis of snow age, snow temperature, and local solar illumination geometry over each pixel in the catchment [*Warren and Wiscombe*, 1980]. This parameterization was shown to be superior to other techniques in distributed snowmelt applications over alpine terrain [*Molotch and Bales*, 2006].

[21] Incoming longwave radiation was estimated using the Idso2 formulation [*Idso*, 1981], with spatially distributed air temperature inputs determined as described above. The spatial estimates of relative humidity, needed for the Idso2 approximation, were derived from air temperature surfaces with specific humidity assumed spatially constant throughout the modeling domain [*Cline et al.*, 1998]. Here specific humidity was calculated from relative humidity and temperature observations at the D-1 station. Longwave emission was estimated using the Steffan Boltzman approximation with an assumed snow emissivity of 0.98 and a snow surface temperature prescribed on a per pixel basis across the catchment as a 2-h lag of air temperature, constrained to 0°C.

3.3.2. Remotely Sensed Snow Cover Data

[22] We acquired remotely sensed imagery from aircraft to estimate SCA on 22 May, 9 June, and 21 July 1996 (i.e., days of year 143, 161, and 203, respectively). SCA estimates were derived at 10-m spatial resolution using manual interpretation of snow-covered and snow-free areas and were resampled to estimate fractional SCA at 30-m resolution. Shaded areas were masked out during classification and were classified separately. These maps were evaluated using visual inspection, and classification was repeated until a good visual match resulted. Glaciers were assumed to overlie talus. In the baseline simulation, only the initial image on 22 May was used to define the snow-covered area; fractional coverage was determined as the number of snow-covered pixels within a given subunit divided by the total number of 10-m pixels within the subunit. In the coupled simulations all of the images were used to construct snow cover depletion curves as described in equation (4).

3.3.3. Snow Depth and Water Equivalent

[23] A snow survey was conducted in the GLV4 prior to maximum snow accumulation (23–25 April 2006), following the general protocols of *Williams et al.* [1999] and *Erickson et al.* [2005]; in 1996 sampling was reduced in scope relative to other years with 11 snow depth measurements recorded (average snow depth was 1.8 m, and the standard deviation was 0.14 m). Snow density was measured in vertical increments of 10 cm using a 1-L (1000 cm^3) stainless steel cutter and an electronic scale (±2 g) at 11 pit locations (average density was 402 kg m^{-3}, and SWE averaged 0.73 m). Observed snow temperatures were below 0°C (average of –2.9°C), suggesting no loss of water or chemical mass from the seasonal snowpack prior to sampling.

3.3.4. Hydrochemical Data

[24] Surface waters (snowpack, stream, lake, and soil lysimeters) were collected as grab samples approximately weekly as part of the Niwot Ridge Long-Term Ecological Research project. All samples were analyzed for major cations and anions, pH, acid-neutralizing capacity (ANC), conductance, NH_4^+, NO_3^-, and dissolved organic nitrogen [see *Williams et al.*, 2001]. These chemical measurements were used within the AHM as concentration values for the specific N species (nitrate and ammonium) in precipitation chemistry input files. These concentration values were then combined with snowfall or rainfall amounts internal to the AHM to calculate chemical loading to the catchment. Soil solution was collected in zero-tension soil lysimeters above Green Lake 4, the same as in the work by *Liu et al.* [2004] and *Williams et al.* [2006]. Release of solutes from the snowpack was investigated by collecting snowpack meltwater in 1-m^2 snow lysimeters before contact with the ground, following the protocol of *Williams et al.* [1996].

[25] Precipitation chemistry was sampled weekly at the Niwot Ridge Saddle Tundra Laboratory as part of the

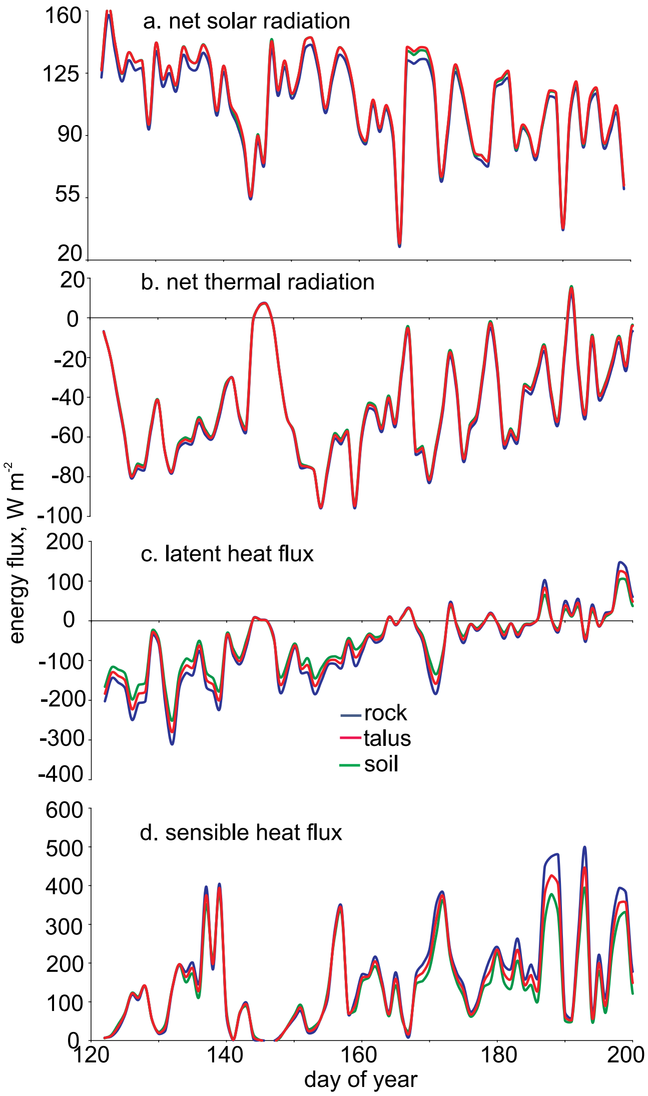

Figure 2. Temporal distribution of basin-wide mean over-snow net (a) solar and (b) thermal radiation and (c) latent and (d) sensible heat fluxes.

National Atmospheric Deposition Program–National Trends Network (Coordination Office, Illinois State Water Survey, 1998, http://nadp.sws.uiuc.edu/). These weekly samples were used to establish the chemical composition of wet (snow and rain) inputs. Dry deposition was calculated for all species by subtracting winter wet deposition from peak accumulation observed in snow pits. Modeled summer N dry deposition was based on the estimate of *Baron and Campbell* [1997], which was 1.3 kg ha^{-1} a^{-1}. All other species in summer dry deposition were left at the values used for AHM simulations in the Emerald Lake catchment [*Wolford et al.*, 1996].

4. Results

4.1. Energy Fluxes

[26] Modeled net thermal and solar radiation were typically opposite in sign. During periods of cloud cover there were sharp decreases in net solar radiation and corresponding increases in net longwave radiation (Figures 2a and 2b); atmospheric emissivity increased during cloudy conditions. Net solar radiation during the modeling period was similar for all three subunits with talus averaging 4 W m^{-2} lower than rock and soil (Table 1); note that statistics reported are for snow-covered areas only. The proportion of net solar radiation to total energy flux for the different subunits was 28% over rock, 32% over soil, and 31% over talus; proportions are based on the net solar radiation values shown in Table 1 divided by the sum of absolute values for all energy terms listed. Average radiative fluxes exhibited subtle variability over the different subunits, with net solar radiation 3% lower over rock subunits relative to soil and talus and net longwave radiation 2% higher over rock versus soil; paired, two-sample-for-means t-tests indicated that mean values were significantly different (P values < 0.01). Within individual subunits, spatial variability in net solar radiation was considerably greater over rock subunits; the coefficient of variation of daily averaged net solar radiation was 21% greater over rock versus soil subunits. Topographic heterogeneity is greater over rock relative to soils.

[27] Sensible heat fluxes were the largest component of the energy balance, with little difference among subunits with respect to season averages; proportions for sensible heat fluxes ranged from 41 to 43% of total energy fluxes (Table 1). Latent heat fluxes were opposite in sign from sensible heat fluxes and varied considerably over the different subunits (Figures 2c and 2d); averaged over the snowmelt season, latent heat fluxes were 26 and 12% greater in magnitude over rock subunits relative to soil and talus subunits, respectively. Differences were most pronounced early in the snowmelt season when drier air conditions and higher wind speeds enhanced latent energy fluxes (Table 1); April modeled latent heat fluxes over rock subunits were 26 and 12% greater in magnitude relative to soil and talus subunits. Conversely, differences in sensible heat fluxes over the different subunits were most pronounced late in the snowmelt season; spatial variability in air temperature gradients between the snow surface and the atmosphere resulted in a 17 and 9% greater amount of seasonal sensible heat exchange over rock versus soil and talus subunits, respectively. Differences were particularly pronounced during July when modeled sensible heat fluxes

Table 1. Mean Monthly and Seasonal Modeled Over-Snow Energy Fluxes for the Different Landscape Units[a]

	Net Solar Radiation			Net Thermal Radiation			Sensible Heat			Latent Heat		
Month	Rock	Soil	Talus	Rock	Soil	Talus	Rock	Soil	Talus	Rock	Soil	Talus
May	120	120	117	−46	−44	−45	96	95	96	−129	−103	−116
June	110	109	106	−54	−52	−53	169	149	159	−55	−41	−48
July	98	97	95	−32	−29	−30	258	195	226	29	19	24
Season	111	111	107	−35	−32	−33	163	139	151	−62	−49	−55

[a]Energy fluxes are in W m^{-2}. Note that net solar radiation corresponds to 0.3–3.5 μm and net thermal radiation corresponds to 3.5–50 μm.

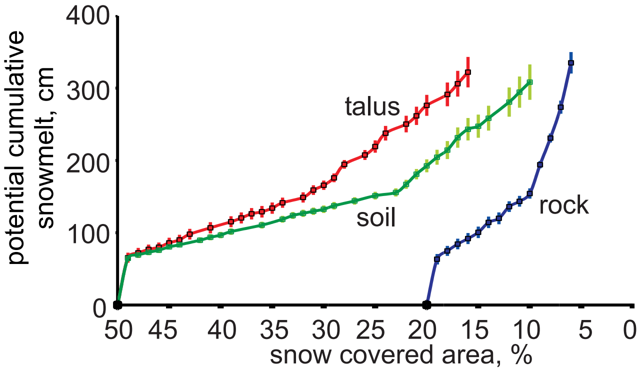

Figure 3. Statistical distribution of potential cumulative snowmelt as a function of snow-covered area over the different subunits. Each point along the curves represents the estimate of snow-covered area averaged over the subunit from equation (4). The vertical bars indicate ±1 standard deviation about the mean (squares) of potential cumulative snowmelt within the subunit. The integration of the area under each curve represents the total snow water equivalent on each subunit.

over rock subunits were 32 and 14% greater than over soil and talus subunits, respectively.

4.2. Snow Cover Depletion and Snowmelt

[28] Figure 3 shows the snow cover depletion curves for rock, soil, and talus subunits. The integral of each of these curves represents the reconstructed SWE for each subunit. Hence, these curves illustrate the considerable differences in snowmelt production and initial SWE for the different subunits. The mean SCA at the beginning of the model run (e.g., day of year (DOY) 122) was 50% on soil and talus subunits and 20% on rock subunits (Figure 3). The average slopes (ΔSCA per centimeter of cumulative melt flux) of the depletion curves were −0.008 for rock, −0.02 for soil, and −0.015 for talus. Hence, snow cover depletion on soil and talus subunits was 150 and 88% more sensitive to melt flux relative to rock subunits, implying a more uniform snow distribution over these subunits. Modeled basin average cumulative potential snowmelt was 4% greater over rock versus talus and 8% greater over rock versus soil (Figure 3). The minimum cumulative potential snowmelt over talus and soil subunits was 5 and 9% less than rock subunits.

[29] Snow cover extent shifted as the snowmelt season progressed, with snow disappearance occurring largely along the margins of continuous snow-covered regions (e.g., Figures 4a and 4b); shallower snow adjacent to deep snow drifts become snow-free earliest. At the end of the snowmelt season snow cover was limited to the glacial subunit and an isolated snowfield within the talus subunit (Figure 4c).

[30] Significant differences in snowmelt over the different landscape units were evident (Figures 4d–4f). Meltwater production over rock subunits was relatively low throughout the modeling period. The dominant subunits contributing meltwater shifted from soil and talus early in the snowmelt season to talus and glacial subunits late in the snowmelt season (Figures 4d–4f). These trends were controlled by both the climatology (i.e., increased air temperatures at lower elevations enhanced sensible and latent heat fluxes) and the heterogeneous distribution of snow at the beginning of the snowmelt season.

[31] The signature of meltwater production for the baseline AHM simulations was distinctly different from the coupled AHM (Figures 5a and 5b). Averaged over the snowmelt season, baseline simulations predicted the greatest amount of snowmelt over soil subunits, 106% greater than talus and 58% greater than rock (Figure 5a). Conversely, average snowmelt for the coupled simulations was greatest for talus subunits at 60% greater than rock and 13% greater than soil (Figure 5b). The proportion of total meltwater production from each subunit contributing to streamflow differed considerably for the baseline and coupled simulations; proportions were determined by weighting the snowmelt by the areal extent of each subunit. Baseline simulations attributed total basin outflow to 46% from soil, 25% from talus, and 29% from rock. Conversely, coupled simulations ascribed the largest meltwater production to talus at 47%, with 37% attributed to soil and 16% attributed to rock subunits. These differences result from the explicit treatment of energy fluxes and snow cover extent by the coupled simulations relative to the implicit approach of the baseline simulations.

4.3. Snow Water Equivalent

[32] Maximum snow water equivalent in the coupled simulations was 94 cm on average over talus subunits, with

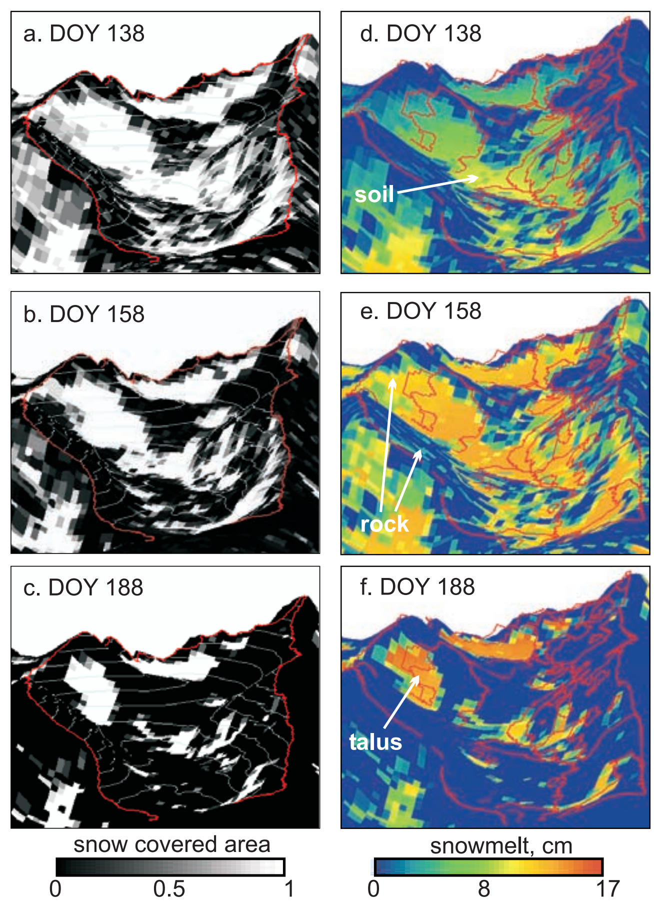

Figure 4. Coupled model estimates of snow cover area on days of year (a) 138, (b) 158, and (c) 188. (d–f) Corresponding coupled model estimates of snowmelt with the outline of the subunit boundaries shown in red.

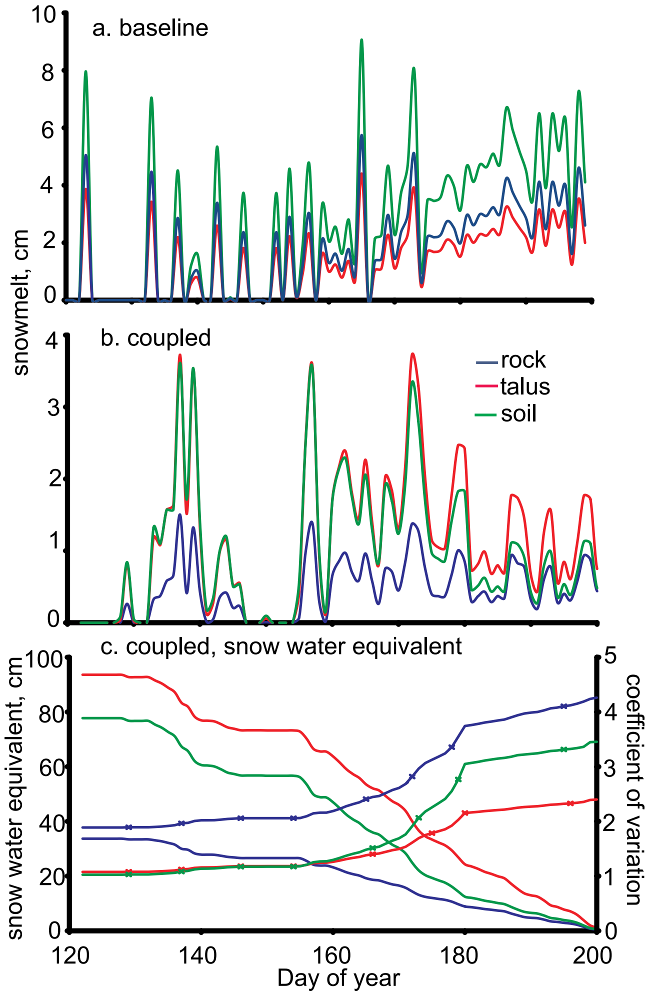

Figure 5. (a) Baseline AHM and (b) coupled model snowmelt time series over the different landscape units within the basin. (c) Time series of daily mean snow water equivalent estimated using the coupled model; the coefficient of variation is also shown with crosses. Lake and glacier subunits are not shown.

soil and rock subunits 17 and 64% lower, respectively. At the onset of the snowmelt season, the coefficient of variation (CV) for the coupled simulations over rock subunits was 78% greater than for talus or soil subunits (Figure 5c). Variability in modeled SWE increased throughout the model run, with proportionally larger increases in variability over soil subunits; the CV reached a maximum at 4.3, 3.5, and 2.4 for rock, soil, and talus subunits, respectively. Averaged throughout the model run, the CV over rock subunits was 75 and 46% greater than for talus and soil subunits, respectively. These differences are somewhat intuitive as rock subunits are restricted to the higher, more topographically heterogeneous portions of the watershed. It is important to note here that SWE distribution was not treated explicitly in the baseline simulations and therefore no SWE statistics are reported for the baseline case.

[33] Comparisons of reconstructed SWE estimates with the observation-based SWE estimates of *Erickson et al.* [2005] showed that spatial variability in SWE was well explained by the model (Figures 6a and 6b). In particular, areas of greater snow accumulation along the western portion of the basin were well recovered by the model as were areas of preferential accumulation along the valley floor and the northeastern quadrant of the watershed.

4.4. Hydrochemical Fluxes

[34] Baseline estimates of discharge were based on direct observations, and therefore discharge estimates of the baseline simulation were more accurate than the uncalibrated coupled simulation (Figure 7a). Modeled discharge explained 95 and 70% of observed streamflow for the baseline and coupled simulations, respectively. Total baseline and coupled model discharge estimates were 2.33 $\times$ 10^4 m^3 and 2.32 $\times$ 10^4 m^3, respectively, overestimating observed discharge (2.22 $\times$ 10^4 m^3) by 4.9 and 4.2%, respectively. Given the calibrated versus uncalibrated nature of baseline

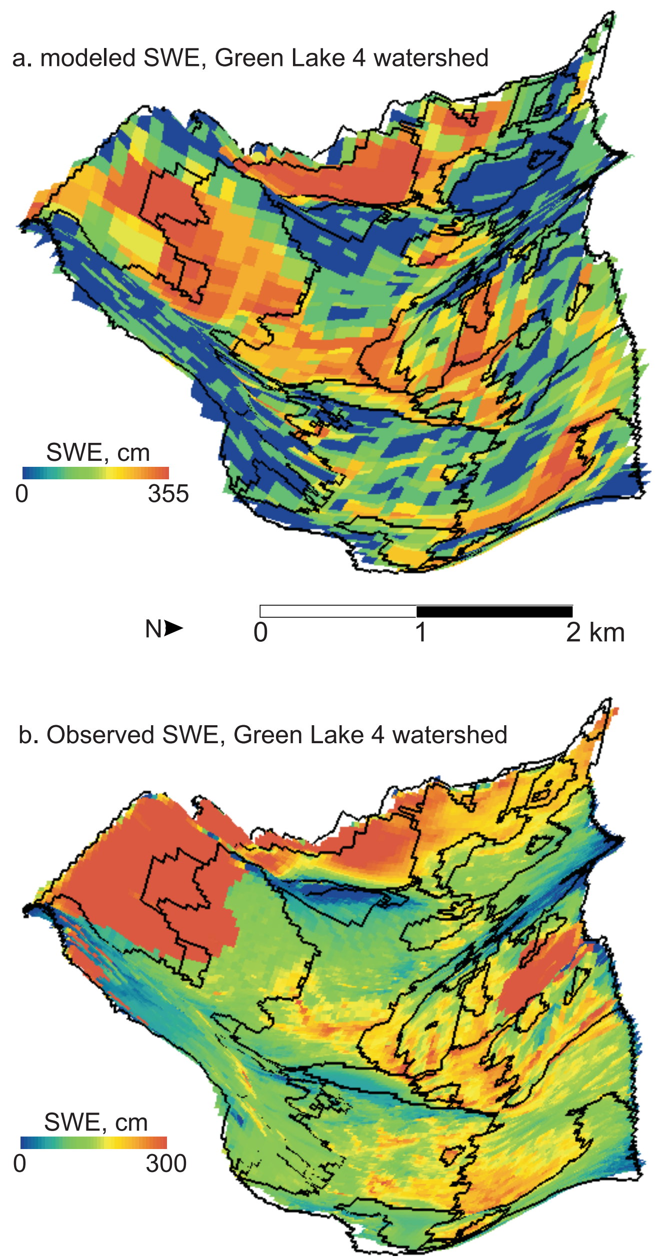

Figure 6. (a) Modeled and (b) observed SWE at maximum accumulation (6 May 2006) in the Green Lake 4 watershed.

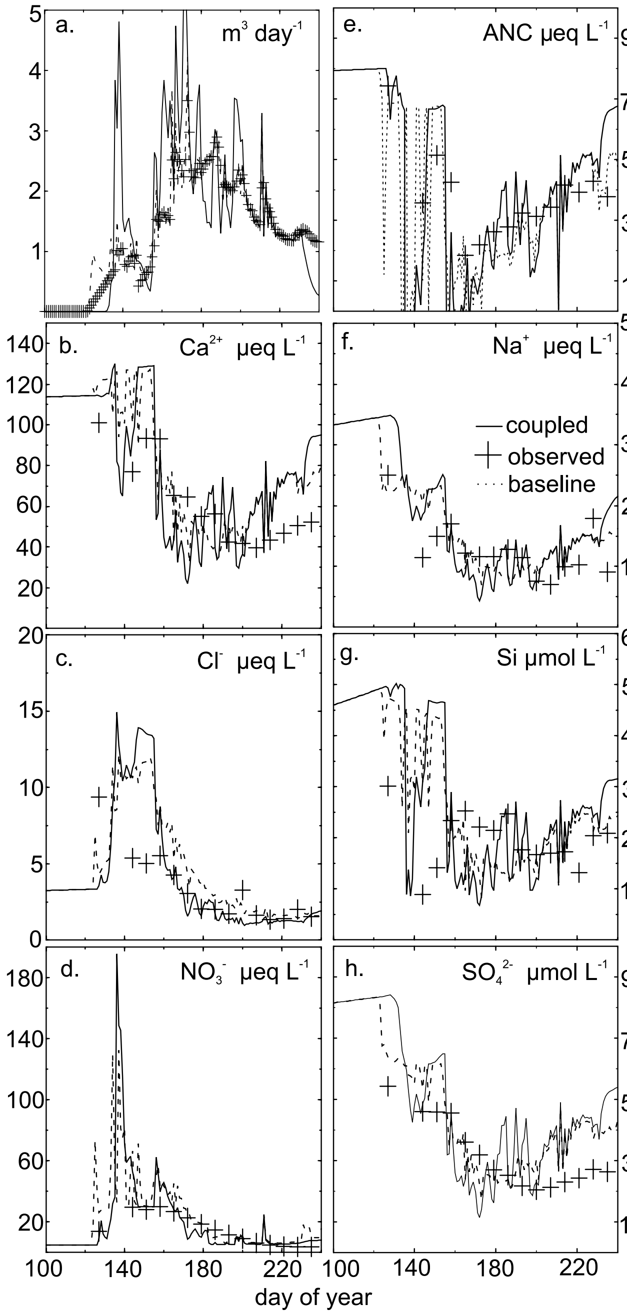

Figure 7. Modeled (a) discharge, (b) calcium, (c) chloride, (d) nitrate, (e) acid-neutralizing capacity (ANC), (f) sodium, (g) silica, and (h) sulfate concentrations at the GLV4 outflow as simulated using the Alpine Hydrochemical Model without (baseline) and with (coupled) a coupled distributed snowmelt model.

and coupled simulations of discharge, the comparison should not be considered a reflection of poor model performance for the coupled simulation but rather a positive reflection on the uncalibrated snowmelt models performance.

[35] Importantly, predictions of stream concentrations for the coupled model outperformed the calibrated baseline simulation. Baseline overpredictions of base cation concentrations during snowmelt (DOY 120 to DOY 220) were partially corrected in the coupled simulations; coupled estimates of Ca^{2+} concentrations were 6% lower than baseline simulations during the snowmelt period (Figure 7b). At the onset of snowmelt (DOY 120 to DOY 150), both baseline and coupled simulations estimated an increase in Ca^{2+} concentration followed by a rapid decrease. Observed concentrations also show these fluctuations with Ca^{2+} concentrations decreasing between DOY 94 and DOY 146, followed by an increase in observed concentrations on DOY 153 before decreasing again as the snowmelt season progressed (Figure 7b). The dynamics of these fluctuations were better approximated with the coupled model, as indicated by the lower value of the coupled simulation on DOY 140. The earlier snowmelt onset date (i.e., DOY 127) in the baseline run resulted in increased Ca^{2+} concentrations which were not mimicked in the coupled simulation until 7 days later (Figure 7b). Toward the end of the snowmelt season (i.e., DOY 200 to DOY 240) Ca^{2+} concentrations were overpredicted by the model in both cases. Over the entire snowmelt season the baseline and coupled models were able to explain 70 and 82%, respectively, (P values < 0.01) of observed Ca^{2+} concentrations.

[36] Baseline model overestimates of Cl^- concentrations were sufficiently corrected by the coupled model; coupled Cl^- concentrations were 10% lower than baseline estimates during the snowmelt season (Figure 7c). While this decrease in simulated Cl^- concentrations indicates overall model improvement, neither model was able to explain the variability in Cl^- concentrations with statistical significance. During peak snowmelt both models overestimated Cl^- concentrations, while the premelt and postmelt periods were both underestimated (see *Meixner et al.* [2000] for a related discussion).

[37] Averaged over the snowmelt season, nitrate concentrations were 12% lower in the coupled versus the baseline simulations (Figure 7d). As a result, the coupled model explained more variability in nitrate concentrations, with 70 versus 83% (P values < 0.01) explained by the baseline and coupled models, respectively. Early in the snowmelt season (i.e., DOY 127) peaks in nitrate predicted by the baseline model were not mimicked in the coupled simulations (Figure 7d). This early season nitrate pulse corresponds with the previously noted discrepancies (section 4.2) in snowmelt onset timing (Figures 5a and 5b) and associated changes in Ca^{2+} and Cl^- concentrations (Figures 7b and 7c).

[38] Averaged over the snowmelt season ANC concentrations were 10% higher in the coupled versus baseline simulations (Figure 7e). Importantly, the coupled model also did not have any negative ANC values, while the baseline model did predict some negative ANC values despite these not being observed in the real system. Additionally, the coupled model explained more variability of the observed system with 72% explained by the coupled model versus only 62% explained by the baseline model.

[39] Model performance for other weathering products, sodium (Na^+) and silica (Si), was significantly worse than for ANC and Ca^{2+}; the coupled simulations did, however, explain more of the Na^+ variability (59 versus 52%) (Figure 7f). Similarly, only 19 and 15% of the variability of Si concentration was explained by the coupled and baseline models, respectively; note that these relationships are not statistically significant. Silica concentrations also increase by 6% in the coupled model versus the baseline model (Figure 7g).

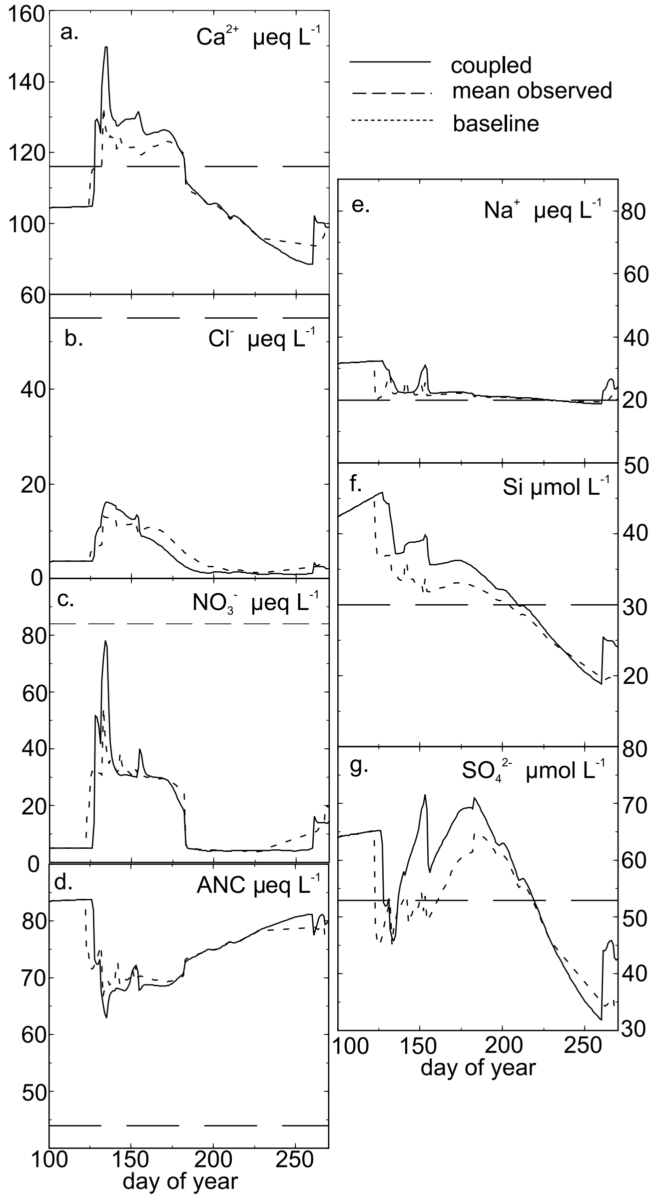

Figure 8. Modeled (a) calcium, (b) chloride, (c) nitrate, (d) ANC, (e) sodium, (f) silica, and (g) sulfate concentrations in the soil subunits as simulated using the Alpine Hydrochemical Model without (baseline) and with (coupled) a coupled distributed snowmelt model. Mean soil chemical observations for a set of soil lysimeters are shown with a horizontal dashed line [*Liu et al.*, 2004].

[40] Finally, the baseline model actually performed better than the coupled model in simulating sulfate concentrations with 75 versus 63% of the variability of sulfate being explained by the baseline versus the coupled model. Also, sulfate concentrations increased in the coupled model by 6% over those observed in the baseline model. This difference likely contributed to the deterioration in model performance since the baseline model overpredicted sulfate concentrations (Figure 7h).

[41] Relative to stream composition, the sensitivity of the chemical composition of the soil solution within the model was much less sensitive to differences in snowmelt in both the coupled and baseline simulations (Figures 8a–8g). Few of the chemical species exhibited more than a 5% deviation from the baseline model. Calcium and Cl- shared a pattern of higher concentrations at peak snowmelt and lower concentrations during the period of decreasing snowmelt in the coupled versus the baseline model (Figures 8a and 8b). Peak soil NO_3-concentrations were 33% higher in the coupled versus the baseline case, approaching the observed NO_3- values (Figure 8c). ANC and Na^+ showed little change between the baseline and coupled models, whereas silica and sulfate had consistently elevated soil chemical concentrations in the coupled model as compared to the baseline model (Figures 8d–8g). Comparisons to mean soil chemical observations at a set of soil lysimeters in the Green Lakes Valley [*Litaor*, 1993] show general agreement for calcium, sodium, silica, and sulfate concentrations (Figures 8a, 8e, 8f, and 8g). However, both the baseline and coupled models significantly underestimated concentrations of chloride and nitrate in the soil solution and overestimated observed soil ANC (Figures 8b–8d). These comparisons with observations must be considered cautiously as measurements of the soil solution were available at only one site within the basin that may not fully represent mean values over the soil subunit.

5. Discussion

[42] In alpine regions, the sensitivity of hydrochemical fluxes to climate variability and change may largely be determined by the relative importance of turbulent and radiative fluxes with respect to snowpack-atmosphere energy exchange. Changes to these hydrometeorological variables act as top down forcings regarding hydrological and biogeochemical sensitivity to climate change. In this regard, increases in regional air temperature in the coming century [*Intergovernmental Panel on Climate Change*, 2007] may increase the relative importance of sensible heat and thermal radiation with respect to snowmelt. These changes may also alter the patterns and timing of snowmelt [*Lundquist and Flint*, 2006]. Similarly, increases in the frequency of dust deposition events may decrease snow surface albedo and increase the relative importance of net solar radiation [*Painter et al.*, 2007]; these processes can be explicitly represented in the coupled model affording scenario analyses related to dust deposition. Multiyear studies are needed to improve our understanding of the processes that control the complex mosaics of the different energy fluxes. The effect of these changes in energy fluxes will propagate through the hydrologic and biogeochemical systems of a catchment, altering the physical, chemical, and biological nature of these ecosystems. What and how large these effects might be can only be estimated through the use of a model that properly represents the important processes in the system; for example, the model applied here includes a physical representation of snowpack fluxes and states such as turbulent exchange, snow cover depletion, and snow surface albedo. Such a process requires us first to improve our predictions of snowmelt and then to investigate how improved representation influences other aspects of integrated alpine catchment modeling.

5.1. Snowmelt Modeling

[43] The small differences in modeled net solar radiation over the different subunits (Figure 2b and Table 1) were

somewhat counterintuitive in that rock subunits are common along the north facing slopes of the basin where solar irradiance is relatively low. Here it is important to recall that the statistics reported are for snow-covered areas only, and therefore it is likely that these similarities result from preferential accumulation and persistence of snow over north facing areas in each of the subunits. Over these north facing areas, decreased solar radiation and preferential deposition of snow from winds blowing out of the southwest extend snow cover duration [*Winstral et al.*, 2002], processes which are implicitly included in the modeling approach.

[44] The estimated proportion of modeled net solar radiation to total radiative exchange over the basin of 0.71 was reasonable relative to previous studies based on observations at alpine sites in the Sierra Nevada, such as the 0.7 reported by *Marks and Dozier* [1992]. The proportion of net solar radiation to total radiative exchange was high relative to the 0.48 reported for observations conducted at the Saddle site on Niwot Ridge during the 1994 snowmelt season [*Cline*, 1997]. Our modeled values reported here include a variety of slopes and aspects, whereas the observations made by *Cline* [1997] were made at a single ridge top site.

[45] The mean basin maximum SWE estimate of 89 cm from the coupled model was only 69% of the 135 cm calculated from the baseline simulation. As a first-order evaluation of these two SWE estimates we refer to the work of *Erickson et al.* [2005], who found statistically significant relationships between observed maximum SWE at the University Camp SNOTEL station and mean snow depth in GLV4. On the basis of these relationships and the maximum SNOTEL SWE in 1996 (88 cm), the mean snow depth in the basin in 1996 was likely greater than 230 cm (as per *Erickson et al.* [2005, Figure 7a]). Prescribing this as the snow depth and solving for snow density, baseline (SWE = 135 cm) and coupled (SWE = 89 cm) simulations of SWE would correspond to snow densities of 587 and 389 kg m^{-3}, respectively, with the coupled value being far more realistic. Furthermore, the 11 snow pit observations in the basin in April 1996 indicate a mean depth of 180 cm, a density of 402 kg m^{-3}, and SWE of 73 cm. Hence, the coupled model SWE estimates are likely more accurate than the calibrated estimates of the baseline simulation. Furthermore, it is important to note that the coupled model is a physically based estimate of SWE distribution whereas the baseline model is based on model calibration against observed streamflow. Hence, the coupled technique is more transferable to ungauged basins and is more suitable for scenario analyses (e.g., climate change).

5.2. Hydrochemical Modeling Implications

[46] Several of the hypotheses outlined by *Meixner et al.* [2000] regarding AHM performance have been addressed under the current research. First, the overprediction of base cation concentrations of the baseline simulations run here and by *Meixner et al.* [2000] was partially corrected using the coupled model. However, the persistent overestimation, despite the larger proportion of water routed through soil and talus subunits, strengthens *Meixner et al.*'s [2000] hypothesis that base saturation levels are too high within the model. Second, *Meixner et al.* [2000] hypothesized that errors in Cl- concentrations may have resulted from poor representation of ionic pulses combined with erroneous routing of concentrated water through the subsurface. This misrepresentation of routing and associated subsurface mixing acts to attenuate the ionic pulse. The combined proportion of soil and talus water was greater for the coupled simulation relative to the baseline simulation, resulting in reduced Cl- concentrations during the snowmelt period (Figure 7c). It remains likely that additional bypass flow associated with the larger snowmelt pulse of the coupled model resulted in diminished contact with the modeled subsurface mixing reservoirs.

[47] During the initial stages of snowmelt (DOY 120 to DOY 155), considerable meltwater production occurred across the catchment (Figure 5b) without a commensurate hydrograph response (Figure 7a), consistent with the hypothesis of *Liu et al.* [2004] that initial snowmelt infiltrated into shallow and/or deep surface reservoirs. Observations and both AHM simulations indicate that ionic concentrations peaked during this period (Figures 7b–7d), suggesting the release of solutes from the snowpack in the form of an ionic pulse and direct input to streamflow. Streamflow during this early snowmelt period was evenly distributed between base flow and snowmelt-derived, infiltration excess overland flow according to *Liu et al.* [2004]. While the majority of meltwater production during this period was produced over talus and soil subunits (according to the coupled snowmelt model) (Figure 5b), *Liu et al.* [2004] showed that talus water contributions to streamflow were particularly low on the basis of mixing model results. Hence, talus water likely infiltrated in the subsurface system, while snowmelt generated over soil subunits was the source of the elevated ionic concentrations observed at the basin outlet. This representation is not included in the current AHM of the basin and indicates that deeper subsurface flow paths with longer residence times may need to be added in the AHM for talus subunits. Additionally, the poor representation of nitrate, chloride, and ANC concentrations in soils by both AHM models indicates that the current representation of soils is not adequate (Figures 8a–8g). Instead, it appears that they are less hydrologically connected than is currently represented. Also, an additional water source representation would likely permit more precise predictions of ANC, chloride, and nitrate in soils by providing a second porous media reservoir. This may lead to more accurate modeling of the soil reservoir and associated stream composition.

[48] The inability to simulate flow accurately in the coupled model indicates that additional storage, likely on the talus subunit, is needed to properly capture hydrologic dynamics in this system. Additional field-based investigations are needed to determine if direct subsurface flow paths exist between talus subunits and the stream whereby ionic pulse-laden waters produced over talus substrates may reach the stream. Hence, the current AHM structure, which routes all meltwater produced over talus subunits through the soil subunits, may need to be revised to include increased storage capacity, longer residence times, and direct routing of water from talus to the stream.

[49] Coupled model estimates of snowmelt during the final phase of the snowmelt season (DOY 155 to DOY 200) were evenly divided between talus and soil subunits early in the period, shifting to mostly talus subunits late in the

snowmelt season (Figure 5b). During this period the base flow contributions to streamflow at the basin outlet decreased dramatically and the proportional contribution of talus and surface water increased according to previous mixing model results [*Liu et al.*, 2004]. The increased surface flow contribution depresses solute concentrations in streamflow (Figures 7b–7d) [*Liu et al.*, 2004]. During this period both surface flow and old water contributions to streamflow may have been derived from meltwater production over talus slopes (Figure 5b); the former generated via saturation excess overland flow, and the latter generated via displacement of old water with snowmelt over talus subunits [*Liu et al.*, 2004]. The persistent snow cover and meltwater production over talus subunits is a new finding relative to previous studies in the basin [e.g., *Meixner et al.*, 2002; *Liu et al.*, 2004] and indicates that improved understanding of flow paths from these subunits may be critical for understanding controls on hydrochemical fluxes during the bulk of the snowmelt season. In this regard, it should be noted that snowmelt contributions to streamflow became increasingly skewed toward talus subunits on DOY 170 (Figure 5b). At the same time, the coupled simulation of nitrate began to underestimate observed concentrations (Figure 7d). This result may indicate that direct flow paths between talus subunits and the stream exist as talus subunits are often an N source [*Williams et al.*, 1998]. Similarly, the baseline simulations, which routed less water over talus subunits than the coupled model (Figures 5a and 5b), exhibited even greater overestimates of nitrate.

[50] Studies of soil contributions of nitrate to streams conducted at Niwot Ridge [*Williams et al.*, 1996] suggest that N sources from the atmosphere may be assimilated, ammonified, and nitrified before reaching streams. The higher peak nitrate concentrations of the coupled versus the baseline model may, therefore, be a result of the timing of snowmelt. The delayed, more rapid onset of snowmelt in the coupled simulation may have mobilized more nitrate by flushing of soils which is incorporated in a limited way within the AHM of the system. Following the onset of snowmelt, immobilization of N within soil subunits may be substantial because of assimilation by subnivean vegetation [*Williams et al.*, 1996], whereas talus, which is devoid of vegetation, may be the dominant source of nitrate to streams. These mechanisms provide an additional explanation of the greater peak nitrate concentration of the coupled simulation, as a greater proportion of source waters were derived from talus versus soil subunits in the coupled simulation (47%) relative to the baseline simulation (25%).

[51] The limited change in soil aqueous phase chemical composition indicates that changes in routing had little effect on soil chemical reactions (Figures 8a–8g). This result is not surprising as soil chemistry is fairly resistant to change, as shown in a variety of acid deposition sensitivity studies over the years [*Chen and Driscoll*, 2005; *Cosby et al.*, 1985a, 1985b]. Thus, the main effect of changing snowmelt rates over different basin subunits in the model is to influence the mixing of waters from different sources (soil versus talus) at different ratios.

[52] The agreements and differences between modeled and observed soil chemical composition indicate that some aspects of soil chemical composition are currently well simulated while others are not. Currently, the soil is represented as uniform and homogenous and is therefore treated as a well-mixed hydrologic and chemical reservoir. These results indicate that this approach may not be entirely appropriate. Large differences in baseline and coupled stream composition and a lack of differences in modeled soil solution composition indicate that the differences in model stream chemistry are due to differences in model flow paths rather than changes in soil or talus solution composition. In as much as the models properly represent processes, this result implies that the real system is more sensitive to changes in routing as opposed to changes in soil solution composition. Additionally, the lack of agreement with observed soil chemical composition for some solutes indicates a need for more complex flow routing schemes in the Green Lakes Valley than is currently represented.

5.3. Implications for Estimating Flow Paths

[53] A key implication of this study is that realistic snowmelt estimates will allow future efforts to improve flow routing and hydrologic process representation within the model. The improved coupled AHM-snowmelt model predictions of chemical composition in coordination with mixture modeling results in this system [*Liu et al.*, 2004] could be used to develop a robust picture of what the flow pathways must be in this system to explain the observed chemical composition. It is likely that these analyses will result in the need to incorporate longer residence time flow paths and increased talus zone storage capacity in the AHM, as discussed in section 5.2, as this has been a prime result of the mixture modeling results to date [*Liu et al.*, 2004]. Without such an improved hydrologic representation, predictions of altered climate or deposition impacts on alpine ecosystems will be ineffective. In order to properly understand the impact of climate variability we need to have a way to link physical changes in snowmelt to changes in hydrologic and chemical flux [*Sickman et al.*, 2001]. Multiyear studies, using the modeling approach illustrated here, are needed to investigate the potential independent and joint impacts of snowmelt timing and increases in atmospheric deposition. While the results presented in this research are likely site- and time period–specific, the reliance on remotely sensed data in the model development and evaluation of model performance ensures transferability of this approach as remotely sensed data become increasingly available. In this regard, this work has implications for applications in other areas and/or studies being performed at the regional scale. Similarly, the coupled modeling approach developed here provides a framework for improving other biogeochemical models [*Li et al.*, 2006; *Tague et al.*, 2004] through spatially explicit snowmelt representation.

6. Conclusions

[54] Improved spatial and temporal estimates of snow water equivalent and snowmelt resulted in improved estimates of chemical concentrations in the Green Lakes Valley and also indicated ways in which the hydrologic and biogeochemical structure of the model could be improved. The study thus demonstrated that improved snowmelt estimates could improve and alter our ideas of how alpine catchment systems function. The magnitude of latent and sensible heat fluxes was largest over rock subunits, particularly late in the snowmelt season, suggesting that snow-

melt sensitivity to future increases in air temperature may be greatest over these subunits. Total basin hydrochemical sensitivity remains unclear as relatively small amounts of meltwater production were derived from rock subunits. Results from the 1-year study conducted here indicated that the distribution of snowmelt shifted from primarily over soil and talus subunits early in the snowmelt season to dominance of talus-derived snowmelt late in the snowmelt season. Total meltwater production from soil, talus, and rock subunits was 46, 25, and 29%, respectively, for the baseline simulation. Conversely, coupled simulations ascribed the largest meltwater production to talus (47%) subunits, with 37 and 16% attributed to soil and rock, respectively.

[55] Accounting for these differences in the AHM reduced model simulations of base cation concentration during snowmelt. Similarly, the coupled model better explained nitrate concentration variability. Early season snowmelt over talus subunits was not detected at the basin outflow but was shown in the coupled model. This result confirms earlier reports that longer residence times and deeper flow paths are needed in catchment biogeochemical models; in particular, more storage capacity in talus areas is needed in the flow path representation of the Green Lakes Valley. The realistic treatment of snowmelt distribution in this situation thus improved model performance but also identified weaknesses in model structure and conception. This result indicates that alternative flow path and residence time conceptions of the Green Lakes Valley need to be tested, a discovery afforded by the explicit representation of snowmelt processes. The incorporation of improved snowmelt estimates in the hydrochemical model has given way to new questions about the hydrologic controls on chemical concentrations and flux. In this regard, we have presented a modeling framework whereby improved estimates of water inputs to the system can be used to constrain source water distributions and fates within the AHM.

[56] **Acknowledgments.** Support for this work was provided by the National Science Foundation Hydrologic Sciences program (EAR-0739107 and EAR-0711600). Additional support was provided by NSF through the Niwot Ridge Long-Term Ecological Research program, NSF EAR-0515592, and EAR-0094312. Support from the Consortium of Universities for the Advancement of Hydrologic Science, Inc. WATERS test bed program (NSF EAR-0610112) is also acknowledged.

References

Baron, J. S., and D. H. Campbell (1997), Nitrogen fluxes in a high elevation Rocky Mountain basin, *Hydrol. Processes*, *11*, 783–799, doi:10.1002/(SICI)1099-1085(199706)11:7<783::AID-HYP519>3.0.CO;2-U.

Baron, J. S., D. S. Ojima, E. A. Holland, and W. J. Parton (1994), Analysis of nitrogen saturation potential in Rocky Mountain tundra and forest: Implications for aquatic systems, *Biogeochemistry*, *27*, 61–82.

Brooks, P. D., and M. W. Williams (1999), Snowpack controls on nitrogen cycling and export in seasonally snow-covered catchments, *Hydrol. Processes*, *13*, 2177–2190, doi:10.1002/(SICI)1099-1085(199910)13:14/15<2177::AID-HYP850>3.0.CO;2-V.

Brooks, P. D., M. W. Williams, and S. K. Schmidt (1996), Microbial activity under alpine snowpacks, Niwot Ridge, Colorado, *Biogeochemistry*, *32*, 93–113, doi:10.1007/BF00000354.

Brooks, P. D., M. W. Williams, and S. K. Schmidt (1998), Inorganic nitrogen and microbial biomass dynamics before and during spring snowmelt, *Biogeochemistry*, *43*, 1–15, doi:10.1023/A:1005947511910.

Brooks, P. D., D. H. Campbell, K. A. Tonnessen, and K. Heuer (1999), Natural variability in N export from headwater catchments: Snow cover controls on ecosystem N retention, *Hydrol. Processes*, *13*, 2191–2201, doi:10.1002/(SICI)1099-1085(199910)13:14/15<2191::AID-HYP849>3.0.CO;2-L.

Caine, N. (1995), Temporal trends in the quality of streamwater in an Alpine environment: Green Lakes Valley, Colorado Front Range, USA, *Geogr. Ann., Ser. A*, *77*, 207–220, doi:10.2307/521330.

Campbell, D. H., D. W. Clow, G. P. Ingersoll, M. A. Mast, N. E. Spahr, and J. T. Turk (1995), Processes controlling the chemistry of two snowmelt-dominated streams in the Rocky Mountains, *Water Resour. Res.*, *31*, 2811–2821, doi:10.1029/95WR02037.

Chen, L., and C. T. Driscoll (2005), Regional assessment of the response of the acid-base status of lake watersheds in the Adirondack region of New York to changes in atmospheric deposition using PnET-BGC, *Environ. Sci. Technol.*, *39*, 787–794.

Cline, D. W. (1997), Snow surface energy exchanges and snowmelt at a continental, midlatitude alpine site, *Water Resour. Res.*, *33*, 689–701.

Cline, D. W., R. C. Bales, and J. Dozier (1998), Estimating the spatial distribution of snow in mountain basins using remote sensing and energy balance modeling, *Water Resour. Res.*, *34*, 1275–1285, doi:10.1029/97WR03755.

Clow, D. W., M. A. Mast, T. D. Bullen, and J. T. Turk (1997), Strontium 87/strontium 86 as a tracer of mineral weathering reactions and calcium sources in an alpine/subalpine watershed, Loch Vale, Colorado, *Water Resour. Res.*, *33*, 1335–1351, doi:10.1029/97WR00856.

Cosby, B. J., R. F. Wright, G. M. Hornberger, and J. N. Galloway (1985a), Modeling the effects of acid deposition: Estimation of long-term water quality responses in a small forested catchment, *Water Resour. Res.*, *21*, 1591–1601.

Cosby, B. J., G. M. Hornberger, J. N. Galloway, and R. F. Wright (1985b), Modeling the effects of acid deposition: Assessment of a lumped parameter model of soil water and streamwater chemistry, *Water Resour. Res.*, *21*, 51–63.

Cumming, B. F., J. P. Smol, J. C. Kingston, D. F. Charles, H. J. B. Birks, K. E. Camburn, S. S. Dixit, A. J. Uutala, and A. R. Selle (1992), How much acidification has occurred in Adirondack region lakes (New York, USA) since preindustrial times, *Can. J. Fish. Aquat. Sci.*, *49*, 128–141.

Daly, C., R. P. Neilson, and D. L. Phillips (1994), A statistical topographic model for mapping climatological precipitation over mountainous terrain, *J. Appl. Meteorol.*, *33*, 140–158, doi:10.1175/1520-0450(1994)033<0140:ASTMFM>2.0.CO;2.

Dozier, J. (1980), A clear-sky spectral solar radiation model for snow-covered mountainous terrain, *Water Resour. Res.*, *16*, 709–718, doi:10.1029/WR016i004p00709.

Dozier, J., and J. Frew (1990), Rapid calculation of terrain parameters for radiation modeling from digital elevation data, *IEEE Trans. Geosci. Remote Sens.*, *28*, 963–969, doi:10.1109/36.58986.

Erickson, T. A., M. W. Williams, and A. Winstral (2005), Persistence of topographic controls on the spatial distribution of snow in rugged mountain terrain, Colorado, United States, *Water Resour. Res.*, *41*, W04014, doi:10.1029/2003WR002973.

Fenn, M. E., et al. (2003), Nitrogen emissions, deposition, and monitoring in the western United States, *BioScience*, *53*, 391–403, doi:10.1641/0006-3568(2003)053[0391:NEDAMI]2.0.CO;2.

Hartman, M. D., J. S. Baron, and D. S. Ojima (2007), Application of a coupled ecosystem-chemical equilibrium model, DayCent-Chem, to stream and soil chemistry in a Rocky Mountain watershed, *Ecol. Modell.*, *200*, 493–510.

Hooper, R. P., and N. Christophersen (1992), Predicting episodic stream acidification in the southeastern United States: Combining a long-term acidification model and the end-member mixing concept, *Water Resour. Res.*, *28*, 1983–1990, doi:10.1029/92WR00706.

Huth, A. K., A. Leydecker, J. O. Sickman, and R. C. Bales (2004), A two-component hydrograph separation for three high-elevation catchments in the Sierra Nevada, California, *Hydrol. Processes*, *18*, 1721–1733, doi:10.1002/hyp.1414.

Idso, S. B. (1981), A set of equations for full spectrum and 8- to 14-μm and 10.5- to 12.5-μm thermal radiation from cloudless skies, *Water Resour. Res.*, *17*, 295–304, doi:10.1029/WR017i002p00295.

Intergovernmental Panel on Climate Change (IPCC) (2007), *Climate Change 2007: The Physical Science Basis: Working Group 1 Contribution to the Fourth Assessment Report of the IPCC*, edited by S. Solomon, D. Qin, and M. Manning, Cambridge Univ. Press, New York.

Jordan, R. (1991), A one-dimensional temperature model for a snow cover, U.S. Army Cold Reg. Res. and Eng. Lab., Hanover, N. H.

Li, X., T. Meixner, J. O. Sickman, A. E. Miller, J. P. Schimel, and J. M. Melack (2006), Decadal-scale dynamics of water, carbon and nitrogen in a California chaparral ecosystem: DAYCENT modeling results, *Biogeochemistry*, *77*, 217–245, doi:10.1007/s10533-005-1391-z.

Liston, G. E. (1999), Interrelationships among snow distribution, snowmelt, and snow cover depletion: Implications for atmospheric, hydrologic, and ecologic modeling, *J. Appl. Meteorol.*, *38*, 1474–1487, doi:10.1175/1520-0450(1999)038<1474:IASDSA>2.0.CO;2.

Litaor, M. I. (1993), The influence of soil interstitial waters on the physicochemistry of major, minor and trace metals in stream waters of the Green Lakes Valley, Front Range, Colorado, *Earth Surf. Processes Landforms*, *18*, 489–504.

Liu, F., M. W. Williams, and N. Caine (2004), Source waters and flow paths in an alpine catchment, Colorado Front Range, United States, *Water Resour. Res.*, *40*, W09401, doi:10.1029/2004WR003076.

Lundquist, J. D., and A. L. Flint (2006), Onset of snowmelt and streamflow in 2004 in the western United States: How shading may affect spring streamflow timing in a warmer world, *J. Hydrometeorol.*, *7*, 1199–1217, doi:10.1175/JHM539.1.

Marks, D., and J. Dozier (1992), Climate and energy exchange at the snow surface in the alpine region of the Sierra Nevada: 2. Snow cover energy balance, *Water Resour. Res.*, *28*, 3043–3054, doi:10.1029/92WR01483.

McConnell, J. R., R. Edwards, G. L. Kok, M. G. Flanner, C. S. Zender, E. S. Saltzman, J. R. Banta, D. R. Pasteris, M. M. Carter, and J. D. W. Kahl (2007), 20th-century industrial black carbon emissions altered Arctic climate forcing, *Science*, *317*, 1381–1384, doi:10.1126/science.1144856.

Meixner, T., and R. C. Bales (2003), Hydrochemical modeling of coupled C and N cycling in high-elevation catchments: Importance of snow cover, *Biogeochemistry*, *62*, 289–308, doi:10.1023/A:1021118922787.

Meixner, T., R. C. Bales, M. W. Williams, D. H. Campbell, and J. S. Baron (2000), Stream chemistry modeling of two watersheds in the Front Range, Colorado, *Water Resour. Res.*, *36*, 77–87, doi:10.1029/1999WR900248.

Meixner, T., L. A. Bastidas, H. V. Gupta, and R. C. Bales (2002), Multicriteria parameter estimation for models of stream chemical composition, *Water Resour. Res.*, *38*(3), 1027, doi:10.1029/2000WR000112.

Meixner, T., J. R. Shaw, and R. C. Bales (2004), Temporal and spatial variability of cation and silica export in an alpine watershed, Emerald Lake, California, *Hydrol. Processes*, *18*, 1759–1776, doi:10.1002/hyp.1416.

Melack, J. M., J. Dozier, C. R. Goldman, D. Greenland, A. M. Milner, and R. J. Naiman (1997), Effects of climate change on inland waters of the Pacific coastal mountains and western Great Basin of North America, *Hydrol. Processes*, *11*, 971–992, doi:10.1002/(SICI)1099-1085(19970630)11:8<971::AID-HYP514>3.0.CO;2-Y.

Molotch, N. P., and R. C. Bales (2005), Scaling snow observations from the point to the grid element: Implications for observation network design, *Water Resour. Res.*, *41*, W11421, doi:10.1029/2005WR004229.

Molotch, N. P., and R. C. Bales (2006), Comparison of ground-based and airborne snow surface albedo parameterizations in an alpine watershed: Impact on snowpack mass balance, *Water Resour. Res.*, *42*, W05410, doi:10.1029/2005WR004522.

Molotch, N. P., T. H. Painter, R. C. Bales, and J. Dozier (2004), Incorporating remotely-sensed snow albedo into a spatially-distributed snowmelt model, *Geophys. Res. Lett.*, *31*, L03501, doi:10.1029/2003GL019063.

Molotch, N. P., M. T. Colee, R. C. Bales, and J. Dozier (2005), Estimating the spatial distribution of snow water equivalent in an alpine basin using binary regression tree models: The impact of digital elevation data and independent variable selection, *Hydrol. Processes*, *19*, 1459–1479, doi:10.1002/hyp.5586.

Mote, P. W., A. F. Hamlet, M. P. Clark, and D. P. Lettenmaier (2005), Declining mountain snowpack in western North America, *Bull. Am. Meteorol. Soc.*, *86*, 39–49, doi:10.1175/BAMS-86-1-39.

Painter, T. H., J. Dozier, D. A. Roberts, R. E. Davis, and R. O. Green (2003), Retrieval of subpixel snow-covered area and grain size from imaging spectrometer data, *Remote Sens. Environ.*, *85*, 64–77, doi:10.1016/S0034-4257(02)00187-6.

Painter, T. H., A. P. Barrett, C. C. Landry, J. C. Neff, M. P. Cassidy, C. R. Lawrence, K. E. McBride, and G. L. Farmer (2007), Impact of disturbed desert soils on duration of mountain snow cover, *Geophys. Res. Lett.*, *34*, L12502, doi:10.1029/2007GL030284.

Rosenthal, W., and J. Dozier (1996), Automated mapping of montane snow cover at subpixel resolution from the Landsat Thematic Mapper, *Water Resour. Res.*, *32*, 115–130, doi:10.1029/95WR02718.

Seastedt, T. R., W. D. Bowman, T. N. Caine, D. McKnight, A. Townsend, and M. W. Williams (2004), The landscape continuum: A model for high-elevation ecosystems, *BioScience*, *54*, 111–121.

Sickman, J. O., A. Leydecker, and J. M. Melack (2001), Nitrogen mass balances and abiotic controls on N retention and yield in high-elevation catchments of the Sierra Nevada, California, United States, *Water Resour. Res.*, *37*, 1445–1461, doi:10.1029/2000WR900371.

Suecker, J. K., J. N. Ryan, C. Kendall, and R. D. Jarrett (2000), Determination of hydrologic pathways during snowmelt for alpine/subalpine basins, Rocky Mountain National Park, Colorado, *Water Resour. Res.*, *36*, 63–75, doi:10.1029/1999WR900296.

Sullivan, T. J., D. F. Charles, J. P. Smol, B. F. Cumming, A. R. Selle, D. R. Thomas, J. A. Bernert, and S. S. Dixit (1990), Quantification of changes in lakewater chemistry in response to acidic deposition, *Nature*, *345*, 54–58, doi:10.1038/345054a0.

Sullivan, T. J., B. J. Cosby, K. A. Tonnessen, and D. W. Clow (2005), Surface water acidification responses and critical loads of sulfur and nitrogen deposition in Loch Vale watershed, Colorado, *Water Resour. Res.*, *41*, W01021, doi:10.1029/2004WR003414.

Tague, C., C. McMichael, A. Hope, J. Choate, and R. Clark (2004), Application of the RHESSys model to a California semiarid shrubland watershed, *J. Am. Water Resour. Assoc.*, *40*, 575–589, doi:10.1111/j.1752-1688.2004.tb04444.x.

Tarboton, D. G., and C. H. Luce (1997), Utah energy balance snow accumulation and melt model (UEB): Computer model technical description and users guide, report, Utah Water Res. Lab., Logan, Utah.

Thornton, P. E., S. W. Running, and M. A. White (1997), Generating surfaces of daily meteorological variables over large regions of complex terrain, *J. Hydrol.*, *190*, 214–251, doi:10.1016/S0022-1694(96)03128-9.

Warren, S. G., and W. J. Wiscombe (1980), A model for the spectral albedo of snow. II: Snow containing atmospheric aerosols, *J. Atmos. Sci.*, *37*, 2734–2745, doi:10.1175/1520-0469(1980)037<2734:AMFTSA>2.0.CO;2.

Williams, M. W., and K. A. Tonnessen (2000), Critical loads for inorganic nitrogen deposition in the Colorado Front Range, USA, *Ecol. Appl.*, *10*, 1648–1665, doi:10.1890/1051-0761(2000)010[1648:CLFIND]2.0.CO;2.

Williams, M. W., P. D. Brooks, A. Mosier, and K. A. Tonnessen (1996), Mineral nitrogen transformations in and under seasonal snow in a high-elevation catchment in the Rocky Mountains, United States, *Water Resour. Res.*, *32*, 3161–3171, doi:10.1029/96WR02240.

Williams, M. W., P. D. Brooks, and T. Seastedt (1998), Nitrogen and carbon soil dynamics in response to climate change in a high-elevation ecosystem in the Rocky Mountains, U.S.A., *Arct. Alp. Res.*, *30*, 26–30.

Williams, M. W., D. Cline, M. Hartman, and T. Bardsley (1999), Data for snowmelt model development, calibration, and verification at an alpine site, Colorado Front Range, *Water Resour. Res.*, *35*, 3205–3209.

Williams, M. W., E. Hood, and N. Caine (2001), Role of organic nitrogen in the nitrogen cycle of a high-elevation catchment, Colorado Front Range, *Water Resour. Res.*, *37*, 2569–2581.

Williams, M. W., M. Knauf, N. Caine, F. Liu, and P. L. Verplanck (2006), Geochemistry and source waters of rock glacier outflow, Colorado Front Range, *Permafrost Periglacial Processes*, *17*, 13–33.

Willmott, C. J., and K. Matsuura (1995), Smart interpolation of annually averaged air temperature in the United States, *J. Appl. Meteorol.*, *34*, 2577–2586, doi:10.1175/1520-0450(1995)034<2577:SIOAAA>2.0.CO;2.

Winstral, A., K. Elder, and R. Davis (2002), Spatial snow modeling of wind-redistributed snow using terrain-based parameters, *J. Hydrometeorol.*, *3, 524–538, doi:10.1175/1525-7541(2002)003<0524:SSMOWR>2.0.CO;2.*

Wolford, R. A., and R. C. Bales (1996), Hydrochemical modeling of Emerald Lake watershed, Sierra Nevada, California: Sensitivity of stream chemistry to changes in fluxes and model parameters, *Limnol. Oceanogr.*, *41, 947–954.*

Wolford, R. A., R. C. Bales, and S. Sorooshian (1996), Development of a hydrochemical model for seasonally snow-covered alpine watersheds: Application to Emerald Lake watershed, Sierra Nevada, California, *Water Resour. Res.*, *32*, 1061–1074, doi:10.1029/95WR03726.

T. Meixner, Department of Hydrology and Water Resources, University of Arizona, Tucson, AZ 85721, USA.

N. P. Molotch, Water and Carbon Cycles Group, Jet Propulsion Laboratory, California Institute of Technology, Mail Stop 300-233, 4800 Oak Grove Drive, Pasadena, CA 91109, USA. (noah.p.molotch@jpl.nasa.gov)

M. W. Williams, Institute for Arctic and Alpine Research and Department of Geography, University of Colorado, Boulder, CO 80302, USA.